

Original Research Article

# Discovery and multi-parametric optimization of a high-affinity antibody against interleukin-25 with neutralizing activity in a mouse model of skin inflammation

Ruth Bone<sup>1,\*</sup>, Brian J. Fennell<sup>1</sup>, Amy Tam<sup>2</sup>, Richard Sheldon<sup>3</sup>, Karl Nocka<sup>3</sup>, Sreeja Varghese<sup>1</sup>, Chew Shun Chang<sup>2</sup>, Heike C. Hawerkamp<sup>4</sup>, Aoife Yeow<sup>4</sup>, Sean P. Saunders<sup>4</sup>, Emily Hams<sup>4</sup>, Patrick T. Walsh<sup>5,6</sup>, Orla Cunningham<sup>7,\*</sup> and Padraic G. Fallon<sup>4,6,\*</sup>

<sup>1</sup>BioMedicine Design, Pfizer, Grange Castle Business Park, Clondalkin, Dublin 22, Ireland, <sup>2</sup>BioMedicine Design, Pfizer, Cambridge, MA, 02139, USA, <sup>3</sup>Inflammation & Immunology, Pfizer, Cambridge, MA, 02139, USA, <sup>4</sup>Trinity Biomedical Sciences Institute, School of Medicine, Trinity College Dublin, Dublin 2, Ireland, <sup>5</sup>National Children's Research Centre, Our Lady's Children's Hospital, Dublin 12, Ireland, <sup>6</sup>Trinity Translational Medicine Institute, Trinity College Dublin, St James's Hospital, Dublin 8, Ireland, and <sup>7</sup>UltraHuman Eight Limited, C/o Kreston Reeves LLP, Kent, CT139FF, UK

Received: July 6, 2022; Revised: August 31, 2022; Accepted: September 18, 2022

## ABSTRACT

**Background:** Interleukin (IL)25 has been implicated in tissue homeostasis at barrier surfaces and the initiation of type two inflammatory signaling in response to infection and cell injury across multiple organs. We sought to discover and engineer a high affinity neutralizing antibody and evaluate the antibody functional activity *in vitro* and *in vivo*. **Methods:** In this study, we generated a novel anti-IL25 antibody (22C7) and investigated the antibody's therapeutic potential for targeting IL25 in inflammation. **Results:** A novel anti-IL25 antibody (22C7) was generated with equivalent *in vitro* affinity and potency against the human and mouse orthologs of the cytokine. This translated into *in vivo* potency in an IL25-induced air pouch model where 22C7 inhibited the recruitment of monocytes, macrophages, neutrophils and eosinophils. Furthermore, 22C7 significantly reduced ear swelling, acanthosis and disease severity in the Aldara mouse model of psoriasiform skin inflammation. Given the therapeutic potential of IL25 targeting in inflammatory conditions, 22C7 was further engineered to generate a highly developable, fully human antibody while maintaining the affinity and potency of the parental molecule. **Conclusions:** The generation of 22C7, an anti-IL25 antibody with efficacy in a preclinical model of skin inflammation, raises the therapeutic potential for 22C7 use in the spectrum of IL25-mediated diseases.

**Statement of Significance:** Statement of Significance: We report the generation of a novel mAb, 22C7, against the cytokine interleukin-25. 22C7 inhibited IL25 *in vitro* and *in vivo* and suppressed skin inflammation in a mouse model of psoriasis. Antibody engineering strategies humanized and optimized the properties of 22C7 for development for clinical use.

**KEYWORDS:** antibody engineering; interleukin-25; skin inflammation; psoriasis

\*To whom correspondence should be addressed. Ruth Bone, BioMedicine Design, Pfizer, Grange Castle Business Park, Clondalkin, Dublin 22, Ireland. [ruth.bone@pfizer.com](mailto:ruth.bone@pfizer.com); Padraic G. Fallon, Trinity Biomedical Sciences Institute, School of Medicine, Trinity College Dublin, Dublin 2, Ireland. [pfallon@tcd.ie](mailto:pfallon@tcd.ie); Orla Cunningham, UltraHuman Eight Limited, C/o Kreston Reeves LLP, Kent, UK. [orla@ultrahuman.net](mailto:orla@ultrahuman.net)

© The Author(s) 2022. Published by Oxford University Press on behalf of Antibody Therapeutics. All rights reserved. For Permissions, please email: [journals.permissions@oup.com](mailto:journals.permissions@oup.com)

This is an Open Access article distributed under the terms of the Creative Commons Attribution Non-Commercial License (<https://creativecommons.org/licenses/by-nc/4.0/>), which permits non-commercial re-use, distribution, and reproduction in any medium, provided the original work is properly cited. For commercial re-use, please contact [journals.permissions@oup.com](mailto:journals.permissions@oup.com)

## INTRODUCTION

Interleukin (IL)25, also known as IL17E, is a member of the structurally related IL17 cytokine family. There are six cytokines in the IL17 family (IL17A, IL17B, IL17C, IL17D, IL17E and IL17F) involved in a number of host defense immune responses, as well as being important regulators of tissue homeostasis, with the aberrant expression of these cytokines eliciting inflammatory responses involved in the pathogenesis of several human autoimmune diseases [1]. IL17 cytokines interact with various cell types, that express different heterodimeric receptor complexes, comprised from five homologous subunits IL17RA to IL17RE, with IL17RA common to all receptors. IL17A was the first family member described and has been extensively studied in the context of evoking pro-inflammatory responses and the potential to target IL17 family cytokines or receptors therapeutically. Antibodies against IL17A (Secukinumab and Ixekizumab) and IL17RA (Brodalumab) have been shown to be efficacious and are approved for treatment of moderate to severe plaque psoriasis, psoriatic arthritis and ankylosing spondylitis [2]. Although IL25 is also a potent initiator of inflammation, its biological activity is distinct from other IL17 family members.

IL25 was originally identified in 2001 by sequence alignment from human genomic sequence data and considered a pro-inflammatory cytokine [3]. Further investigation demonstrated IL25 as a type 2 cytokine produced by CD4<sup>+</sup> T-helper (Th) 2 cells, stimulating the secretion of the cardinal Th2 cytokines IL4, IL5 and IL13 [4]. IL25 is a potent inducer of type 2 inflammation, which involves the development of both innate and adaptive type-2 cellular responses, and is associated with the development of asthma and allergy [5]. Mice injected with IL25 developed all the classical hallmarks of type 2 inflammation with marked Th2 cell expansion, eosinophilia, mastocytosis, goblet cell hyperplasia and elevated IgE [4]. The generation of IL25 deficient mice confirmed its role in the generation of functional type 2 immunity, with delayed rejection of the type 2 inducing parasite *Nippostrongylus brasiliensis* [6]. IL25 was also shown to induce the expansion of group 2 innate lymphoid cells (ILCs) with subsequent ILC2 secretion of IL4, IL5, IL9 and IL13 shown to orchestrate adaptive type 2 immunity in the skin, lungs and intestine [6]. In addition to release from immune cells, IL25 is secreted by nonhematopoietic cells, including keratinocytes in the skin as well as epithelial cells in the lung and gut, in a similar manner to IL33 or thymic stromal lymphopoietin (TSLP). The release of these three alarmin cytokines from nonhematopoietic cells acts to initiate the genesis of a type 2 inflammation cascade, with activation of ILC2 and the expansion of Th2 cells and downstream allergic responses including eosinophilia, goblet cell hyperplasia and IgE production. Therefore, IL25 maintains tissue homeostasis at barrier surfaces in the steady state and, in response to infection or cell injury, functions to initiate innate and adaptive immune responses. Although the use of antibodies to target TSLP in severe asthma has recently been approved by the The Food and Drug Administration (FDA) and clinical trials for IL33 are underway, new biologics to target the activity of IL25 need to be developed [7, 8].

Mice deficient in IL25 have been extensively studied and confirm IL25's functional role in type 2 inflammation in various organs, in particular the lung, skin and intestine. Furthermore, mice deficient in the IL25-specific receptor IL17RB (IL25 signals via a heterodimeric IL17RA-IL17RB receptor complex) also have impaired type 2 immune responses. These data on the functional role of IL25 in mouse models, in addition to its expression pattern in human disease states, suggest the potential for IL25 targeting to modulate inflammatory disease [5]. A number of antibodies against IL25 have been generated and shown to effectively modulate inflammation in several preclinical mouse models, including allergic lung inflammation, intestinal inflammation and skin inflammation [9–12]. More recently, a new anti-IL25 antibody, termed LNR125, was shown to suppress not only type 2 inflammation in preclinical models of lung inflammation, as well *in vivo* using human bronchial epithelial cells from patients with asthma, but blocking of IL25 alerted type I/III interferon production and impacted on viral immunity indicative of potential for targeting IL25 to manage viral asthma exacerbations [13]. In the skin, IL25 is expressed by keratinocytes, which also express IL17RA and IL17RB, and can act in an autocrine loop to regulate the proliferation, differentiation and functionality of keratinocytes in initiating inflammatory cascades [10, 11]. Indeed, patients with atopic dermatitis and psoriasis have altered IL25 expression in the skin, consistent with roles in type 2 immunity and IL17-mediated cutaneous inflammation.

To validate the therapeutic potential of IL25-targeting, we generated a high affinity, human/mouse cross-reactive antibody against IL25. *In vitro* characterization of the parental molecule 22C7 demonstrated similar affinity for human (76 pM) and mouse (48 pM) IL25 using BIAcore, and similar potency against human (103 pM) and mouse (71 pM) IL25 in a growth-regulated oncogene alpha (GRO $\alpha$ ) neutralization assay. 22C7 was subsequently shown to inhibit cell recruitment to subcutaneous air pouches in an IL25-dependent cellular infiltration mouse model, in a dose-dependent manner. Furthermore, 22C7 significantly ameliorated the development of pathology in the Aldara model of psoriasis-like skin inflammation. With this proof-of-concept validation of therapeutic efficacy of 22C7, antibody engineering efforts were undertaken to humanize and optimize the properties of 22C7 to facilitate further development as a potential therapeutic molecule.

## RESULTS

### Characterization of hybridoma clone 22C7

*In vivo* immunization of BALB/c mice with recombinant human IL25 identified a panel of anti-IL25 antibodies from which clone 22C7 was chosen for further characterization due to its apparent high affinity binding to both human and mouse target in preliminary screening enzyme-linked immunosorbent assays (ELISAs) (data not shown). Surface plasmon resonance (SPR) was carried out to establish the accurate 1:1 binding kinetics of 22C7 for human and mouse

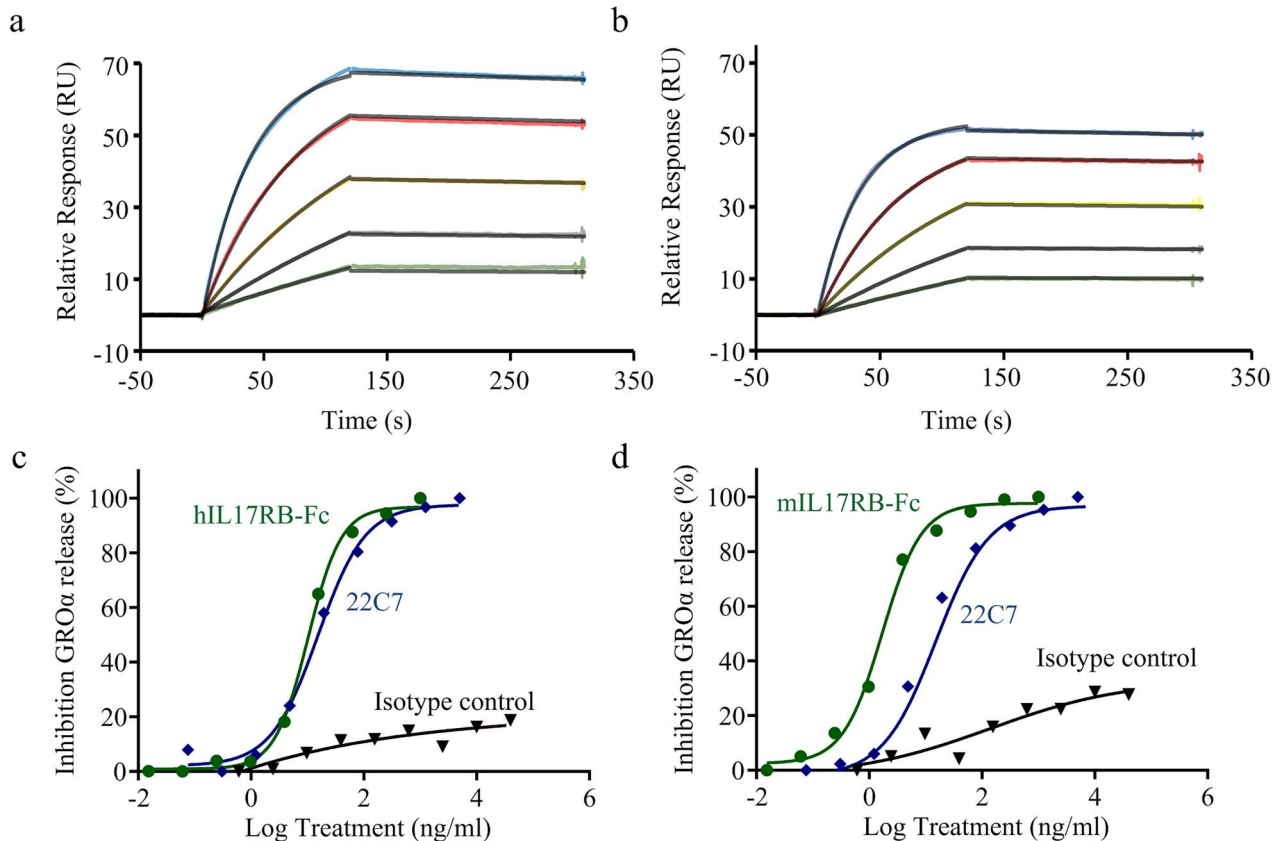


**Figure 1.** Characterization of clone 22C7. The BIAcore T200 was used to determine 1:1 binding kinetics for 22C7 binding to human (a) and mouse (b) IL25. The overlaid sensorgrams in each case represent a dilution series of IL25 concentrations from 25 to 0.78 nM. The relationship between affinity of interaction and potency of neutralization was explored in a HT29 IL25-induced GRO $\alpha$  secretion assay. 22C7 neutralized human (c) and mouse (d) IL25-induced chemokine release with similar potency to a soluble form of the IL17RB receptor.

IL25 using immunoglobulin G (IgG) captured on a BIAcore sensor chip. A dose-dependent response was evident for both human and mouse IL25, with IL25 exhibiting fast association and slow dissociation from 22C7. The  $K_D$  for human IL25 was calculated at 76 pM (Fig. 1a), with a slightly tighter affinity for mouse IL25 at 48.5 pM (Fig. 1b).

The relationship between affinity for target and neutralization potency was assessed using a GRO $\alpha$  signaling assay in HT29 cells, which express the heterodimeric IL17RA-IL17RB complex and respond to exogenous addition of IL25. Cells were stimulated with human or mouse IL25, and 22C7 was assessed for neutralization activity using soluble IL17RB-Fc fusion protein as a positive control. Robust dose-dependent inhibition of GRO $\alpha$  secretion was observed for 22C7, comparable to that for the soluble receptor, confirming its ability to compete for the IL25 receptor binding site. The  $IC_{50}$  for human IL25 was determined to be 103 pM (Fig. 1c) and 70.9 pM for mouse IL25 (Fig. 1d). The characteristics of clone 22C7 are summarized in Table 1.

#### Validation of 22C7 functional activity *in vivo*

With positive data for 22C7 inhibiting IL25 activity *in vitro*, we sought to confirm that the antibody was active *in vivo*. We exploited the propensity of IL25 injection in mice to elicit potent local recruitment of inflammatory cells such

as neutrophils, eosinophils, lymphocytes and monocyte/macrophages [4, 11]. This IL25-mediated sub-cutaneous air-pouch model was used to evaluate 22C7 inhibition of IL25 (Fig. 2a). As expected, the injection of IL25 into established air pouches on the backs of mice elicited significant infiltration of cells into the air pouch 24 h later. Cell recruitment to the air pouch was not altered by mice receiving the mouse IgG2a isotype control (1 000  $\mu$ g) antibody (Fig. 2b). Flow cytometry analysis of cells in the air pouch confirmed that IL25 induced the recruitment of lymphocytes (CD3<sup>+</sup> T cells and CD19<sup>+</sup> B cells), monocyte/macrophages (CD3<sup>-</sup>, CD19<sup>-</sup>, CD11b<sup>+</sup>, Ly6G<sup>low</sup>), neutrophils (CD11b<sup>+</sup>, Ly6G<sup>+</sup>) and eosinophils (CD3<sup>-</sup>, CD19<sup>-</sup>, CD11c<sup>-</sup>, Siglec-F<sup>+</sup>) (Fig. 2(c), Fig. S1). Mice injected with the higher dose of 22C7 (1 000  $\mu$ g) had limited IL25-elicited cell recruitment, with significantly less cells ( $p < 0.001$ ) compared with isotype control-treated mice (Fig. 2b). The activity of 22C7 was dose-dependent, with animals receiving the lower 250  $\mu$ g dose of 22C7 having comparable IL25-induced cell infiltration as isotype control antibody-treated mice (Fig. 2c). These data confirm that 22C7 inhibits the functional activity of IL25 *in vivo* to impair cellular recruitment.

The air pouch model provided preliminary data demonstrating *in vivo* 22C7 activity; however, it requires an exogenous treatment with IL25. For this reason, 22C7 was subsequently tested for efficacy in a more complex model of skin inflammation. We selected the Aldara-induced

**Table 1.** Affinity and potency of parental clone 22C7

	BIAcore			HT29 GRO $\alpha$
	k <sub>a</sub> (1/Ms)	k <sub>d</sub> (1/s)	K <sub>D</sub> (pM)	IC <sub>50</sub> (pM)
Human IL25	2.06E+06	1.56E-04	76	103
Mouse IL25	2.35E+06	1.14E-04	48.5	70.9

Binding kinetics for parental clone 22C7 to human and mouse IL25 was investigated by BIAcore, rate constants were calculated using a 1:1 binding model (T200 Evaluation Software) and the equilibration dissociation constant (K<sub>D</sub>) was calculated as kd/ka. GRO $\alpha$  assay was used to measure 22C7 neutralization of human and mouse IL25 by inhibition of IL25-induced GRO $\alpha$  release, expressed as 22C7 IC<sub>50</sub>

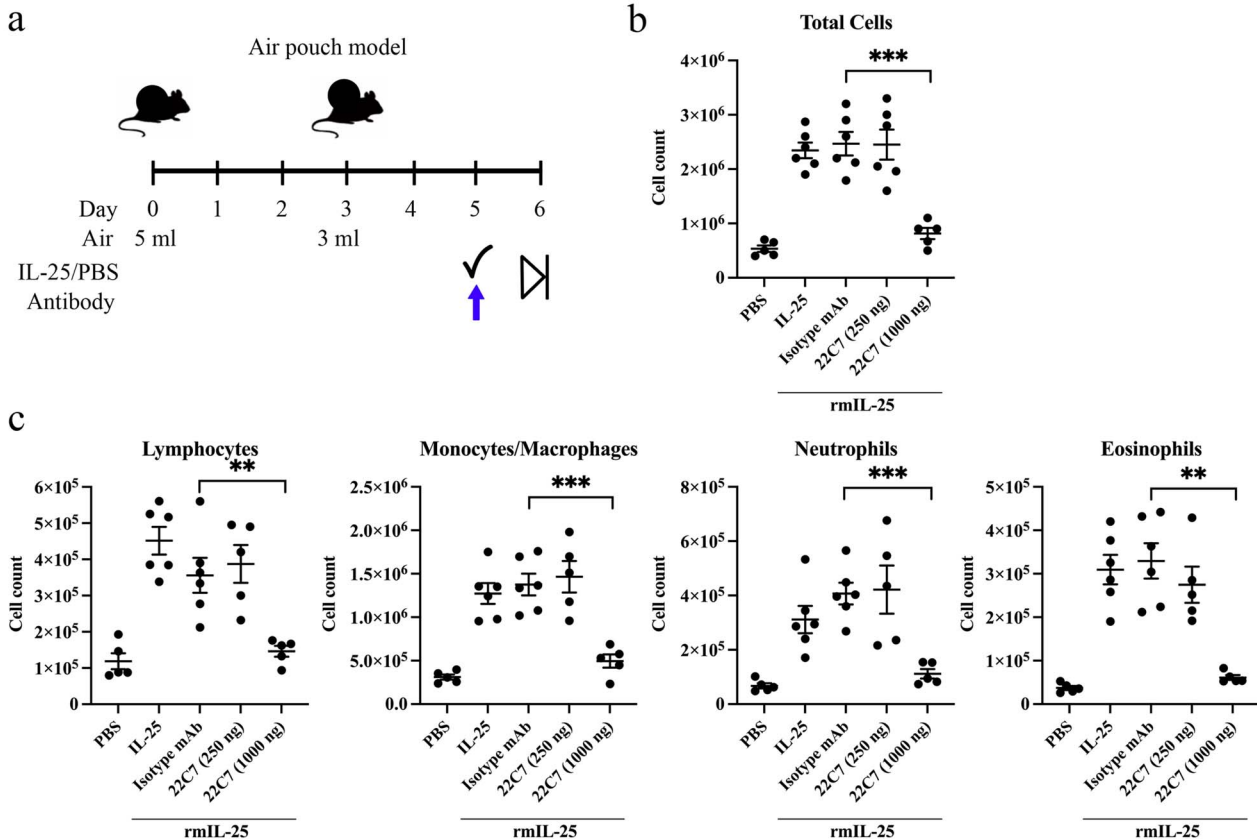


**Figure 2.** Efficacy of 22C7 in a murine air pouch model of IL-25 induced cell infiltration. (a) Schematic of procedure; mice were injected with 5 mL sterile air on Day 0, at Day 3, the air pouch was reinflated with 3 mL sterile air. On Day 5, IL25 or PBS alone was injected into air pouches followed by PBS, 22C7 (250 or 1 000 ng) or isotype control antibody (1 000 ng). On Day 6, air pouches were lavaged and cells recovered. (b) Total live cell counts in the air pouch under the different treatments. (c) Flow cytometry analysis of infiltrated cells: lymphocytes (CD3<sup>+</sup>, CD19<sup>+</sup> cells), monocytes/macrophages (CD3<sup>-</sup>, CD19<sup>-</sup>, CD11b<sup>+</sup>, Ly6G<sup>low</sup>), neutrophils (CD11b<sup>+</sup>, Ly6G<sup>+</sup>) and eosinophils (CD3<sup>-</sup>, CD19<sup>-</sup>, CD11c<sup>-</sup>, Siglec-F<sup>+</sup>). Data are representative of duplicate experiments,  $n = 5-6$  per group. Statistical analysis was carried out using unpaired Student's  $t$ -test:  $p < 0.01$  equals \*\*,  $p < 0.001$  equals \*\*\*

model of psoriasis-like skin inflammation, where the inflammation has been shown to be IL25 mediated [11]. The ears of mice were topically treated daily with Aldara (IMQ 5%) for 12 days. When signs of psoriasis-like inflammation were evident from Day 3, mice received an intraperitoneal (IP) injection of 22C7 or an isotype control antibody (20 mg/kg) every second day (Fig. 3a). Aldara treatment of the mice caused a progressive increase in ear thickness (Fig. 3b and c). Skin inflammation was quantified using a mouse psoriasis area severity index (PASI) system, with elevated PASI scores over the 12 days of treatment (Fig. 3d and e). Mice therapeutically treated with 22C7 from Day 3, when ear thickness was increasing,

had less marked increases in ear thickness from Day 8, with significantly ( $p < 0.001$ ) reduced ear thickness over the course of Aldara treatment compared with the isotype control group (Fig. 3b and c). The signs of psoriasis-like skin inflammation on the ears were also reduced from Day 8 in 22C7-treated animals, with significantly ( $p < 0.001$ ) lower PASI scores relative to control animals (Fig. 3d and e). Furthermore, histological analysis on Day 12 demonstrated that the increase in epidermal thickness, acanthosis and cell infiltrates in the ears of Aldara-treated mice was markedly reduced in 22C7 injected animals relative to isotype control mice (Fig. 3f), with significant reductions in epidermal thickness ( $p < 0.0001$ ; Fig. 3g) and

cell infiltration of the skin ( $p < 0.01$ ; Fig. 3h) of mice treated with 22C7 compared with the isotype controls group.

### Humanization and optimization of 22C7

With validation of the *in vivo* activity of 22C7 in the skin inflammation model, we sought to further engineer this antibody for potential therapeutic use. A complementarity determining region (CDR)-grafting approach was used to humanize 22C7. The murine  $\nu$ -gene regions of 22C7 were identified and compared with annotated human germline V-gene sequences in the IMGT database. Consideration was given to the level of sequence homology between the murine and human sequences but also the biophysical characteristics of these acceptor frameworks, i.e., acceptable expression yields and stability, were also a factor in framework selection. Based on this analysis, the VH CDRs of 22C7 were grafted onto three different VH-3 frameworks: VH3-7, VH3-23 and VH3-30, in addition to three distinct VH-4 members: VH4-30-4, VH4-39 and VH4-59. The VL CDRs of 22C7 were grafted onto three light chain acceptor frameworks: V $\kappa$ 1-33, V $\kappa$ 1-39 and V $\kappa$ 3-11. The resulting VH [6] and VL [3] genes were sub-cloned and combined in a matrix fashion, resulting in 18 framework grafts. These grafts were expressed as IgG, purified and compared with the parental 22C7 IgG in a number of characterization assays. The workflow for this humanization approach is summarized in Fig. S2.

All grafts retained similar binding ( $EC_{50}$ ) and neutralization activity ( $IC_{50}$ ) to the parental 22C7 in the IL25 binding ELISA and GRO $\alpha$  secretion assay, respectively (representative data for the V $\kappa$ 1-39 grafts are shown in Fig. 4a and b; data for all grafts are summarized in Table 2). This maintenance of activity suggested optimal presentation of the 22C7 CDR loops in the prioritized acceptor frameworks. However, analytical size exclusion chromatography (SEC) of the purified IgGs showed that although 15/18 grafts retained  $> 90\%$  peak of interest (POI), comparable to 22C7, the VH3-30 grafts performed poorly at only  $\sim 75\%$  POI (Fig. 4c). As these clones also had significantly lower expression titers (Table 2), they were excluded from further characterization. Increasingly, favorable antibody developability characteristics are considered essential for therapeutic development and have been correlated with progression to late-stage development [14]. For this reason, a series of developability assays were carried out on the remainder of the grafts to allow differentiation between clones and enable selection of a final humanized graft. Thermal stability of the grafts was assessed using differential scanning calorimetry (DSC) with all displaying Fab  $T_m$  values higher than the parental 22C7 (Fig. 4d and Table 2). Deoxyribonucleic acid (DNA) and insulin specificity ELISAs and assessment of aggregation propensity using an affinity-capture self-interaction nanoparticle spectroscopy (AC-SINS) assay demonstrated that all grafts had exemplary properties with scores of  $\leq 3.0$  in all cases, predicting a standard platform process for any subsequent antibody development [15]. Finally, the humanized graft sequences were subjected to an *in silico* assessment of potential immunogenicity using Epivax epitope prediction software [16]. Based on the cumulative functional and biophysical characterization, the

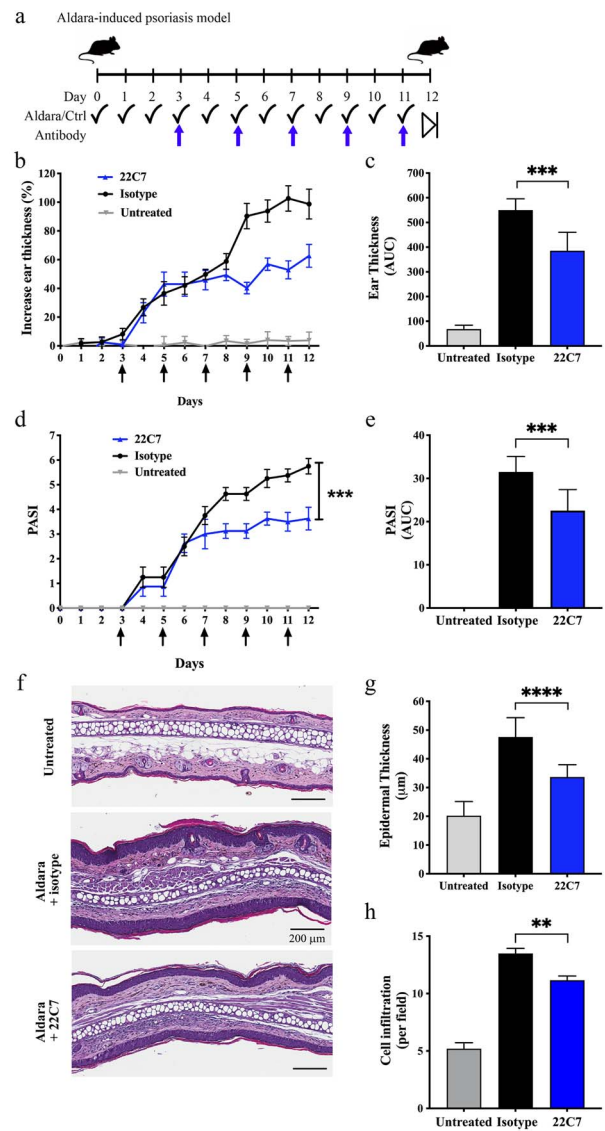


**Figure 3.** Evaluation of 22C7 in Aldara model of psoriasis-like skin inflammation. (a) Schematic of procedure; the ears of mice were treated daily with Aldara cream for 11 days. From Day 3, mice received the 22C7 antibody or isotype control antibody (20 mg/kg) every other day. (b) The ear thickness was measured daily and data displayed as percent increase compared with the initial ear thickness. (c) Increase in ear thickness of individual mice during the course of treatments displayed as AUC. (d) Mouse PASI during the course of the experiment. (e) Mouse PASI score of individual mice expressed as AUC. (f) Histology of ears of untreated mice and Aldara-treated animals receiving 22C7 or isotype control antibody. Magnification:  $\times 10$ , Scale bar: 200  $\mu\text{m}$ . (g) Epidermal thickness of mouse ears as a measure of acanthosis. (h) Dermal cell infiltration, expressed as cells per field of view. Data are representative of three separate experiments,  $n = 5-8$  mice per group. Statistical differences between Aldara-treated groups were analysed using an unpaired Student's  $t$ -test:  $p < 0.01$  equals \*\*,  $p < 0.001$  equals \*\*\*,  $p < 0.0001$  equals \*\*\*\*.

VH3-23/V $\kappa$ 1-39 graft was selected as the final humanized molecule, maintaining equivalent functional activity to the parental 22C7, and displaying the favorable developability characteristics required for therapeutic progression, including low predicted immunogenicity.

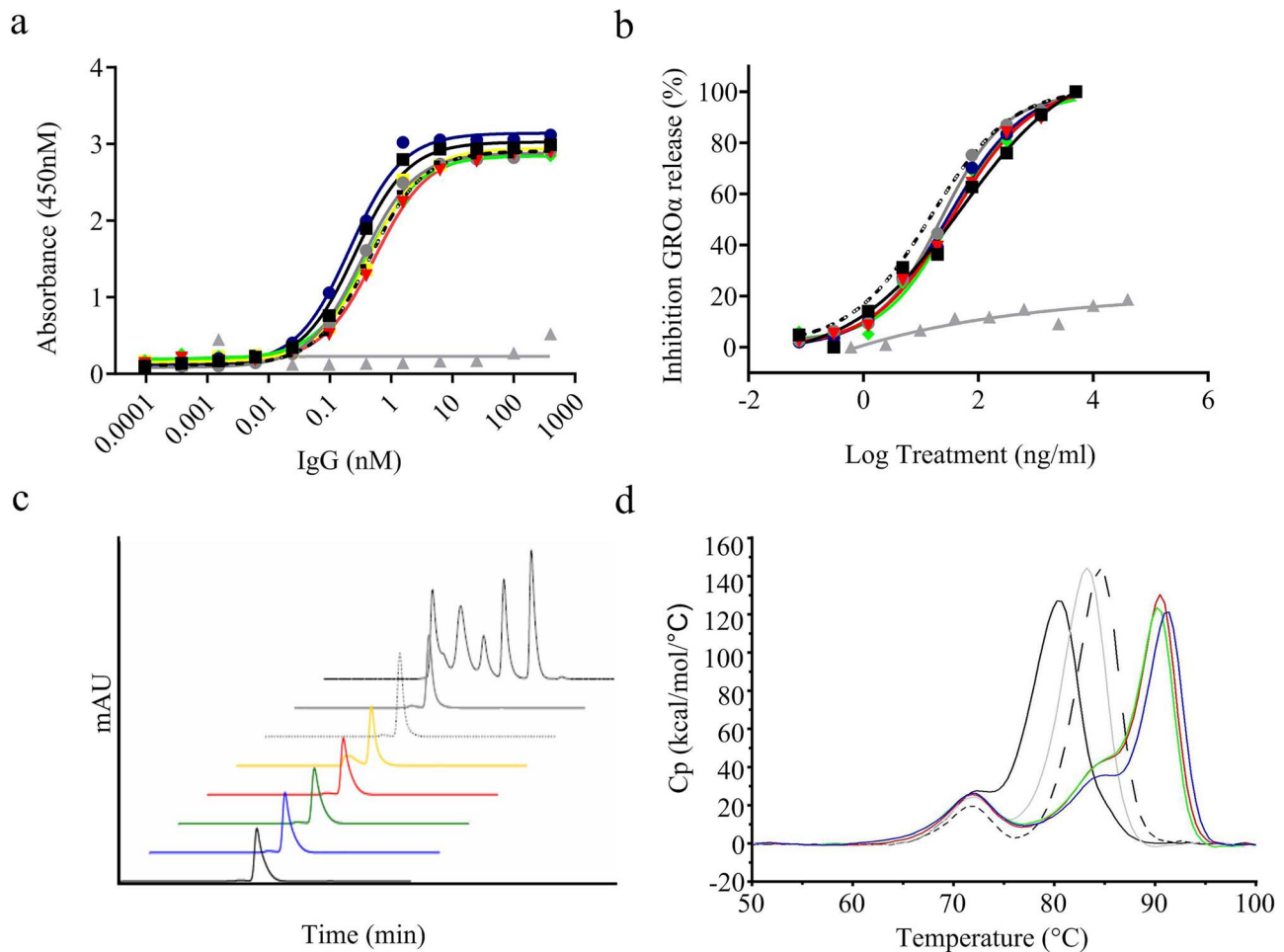


**Figure 4.** Characterization of humanized grafts of 22C7. Representative graphs show data generated for the light chain  $V\kappa$ 1–39 grafts in combination with VH3–23 (black dotted line), VH4–30 (red), VH3–7 (grey circles), VH4–59 (blue), VH4–39 (green), VH3–30 (yellow) compared with parental 22C7 (black squares) and negative isotype control (grey triangles). All grafts retained comparable binding to human IL25 (a) and inhibition of IL25-induced GRO $\alpha$  secretion (b). (c) Analytical SEC confirmed that the VH3–30 combinations suffered from the presence of high molecular weight aggregates resulting in a lower % POI. (d). DSC analysis demonstrated higher thermal stability for the humanized grafts compared with parental 22C7.

## DISCUSSION

The cytokine IL25 is an important mediator of type 2 immunity, orchestrating cells involved in both the innate and adaptive responses. This role in type 2 immunity also implicates IL25 in the pathogenicity of inflammatory and allergic diseases. Indeed, IL25 has roles in asthma, skin inflammation and inflammatory bowel disease, viral infections, cancer and several autoimmune conditions including rheumatoid arthritis, type 1 diabetes, multiple sclerosis, systemic lupus erythematosus and Sjögren's Syndrome as well as metabolic disorders [5, 17, 18]. Therefore, the generation of a functional neutralizing antibody to IL25 could have significant clinical benefit in a number of human inflammatory diseases.

Herein we show the generation of a functional antibody against IL25, clone 22C7, which demonstrates high affinity binding to both mouse and human IL25, as demonstrated by SPR and *in vitro* neutralization assay. These characterization assays confirmed the ability of 22C7 to effectively bind to both mouse and human IL25, with rapid association and slow dissociation. The ability of 22C7 to neutralize

exogenous IL25 *in vitro* as determined by GRO $\alpha$  secretion by IL17RA-IL17RB complex expressing HT29 cells was comparable to that exhibited by the positive control of soluble IL17RB-Fc fusion protein, confirming the efficacy of 22C7 to bind to and neutralize IL25. To date no IL25 targeting molecule has proceeded to clinical studies, although recently an antibody targeting IL25 has demonstrated pre-clinical efficacy in a lung inflammation model [13]. *In vitro* characterization of this molecule reports single-digit pM affinity and IC<sub>50</sub> potency in the 500–1 000 pM range, 22C7 compares favorably to this molecule demonstrating similar affinity and superior potency values.

To determine the efficacy of 22C7 to attenuate the functional activity of IL25 *in vivo*, we used two distinct mouse models. First, air pouch studies in mice were performed harnessing the air pouch as a model in which to study cellular recruitment elicited *in vivo* by IL25. Injection of 22C7 dose-dependently significantly reduced the IL25-induced recruitment of immune cells into the air pouch, confirming the ability of 22C7 to effectively neutralize exogenous IL25. Second, to confirm this *in vivo* activity

**Table 2.** Characterization of humanized grafts of 22C7

Clone (VH/VK)	Titer (mg/L)	Fab Tm (°C)	POI (%)	Polyreactivity AC- SINS/D- NA/Insulin	Epivax score	ELISA EC <sub>50</sub> (nM)	K <sub>D</sub> human (pM)	K <sub>D</sub> mouse (pM)	IC <sub>50</sub> GRO $\alpha$ (pM)
22C7 (parental)	24	80.3	97	1/1/1	21.57	0.258	116	50	340
3-23/1-39 (selected graft)	32	85.07	97	1/2/1	-55.08	0.4488	86	70	100
3-23/1-33	35	87.6	97	1/2/2	-42.77	0.3632	97	50	175
3-23/3-11	25	84.76	95	1/2/1	-43.54	1.352	81	69	308
3-7/1-39	33	83.63	96	1/2/2	-57.63	0.3288	87	51	154
3-7/1-33	35	86.53	97	1/2/2	-44.72	0.3182	92	44	102
3-7/3-11	33	84.1	97	2/2/2	-46.09	0.3863	85	50	142
4-30-4/1-39	26	90.32	97	1/3/2	-11.8	0.5448	145	75	238
4-30-4/1-33	27	92.99	96	1/3/3	1.1	0.4116	140	82	208
4-30-4/3-11	27	89.24	97	1/3/3	-0.27	0.4963	165	88	119
4-39/1-39	28	90.09	97	1/3/2	-13.14	0.4011	153	90	235
4-39/1-33	28	92.84	94	1/3/3	-0.23	0.5966	175	98	202
4-39/3-11	16	89.09	94	1/3/3	-1.6	0.5907	200	109	229
4-59/1-39	28	90.92	97	1/3/2	-13.49	0.2115	118	62	198
4-59/1-33	27	93.46	96	1/3/3	-0.59	0.6866	130	89	246
4-59/3-11	24	89.58	95	2/3/3	-1.96	0.2585	139	86	152
3-30/1-39	11	-	76	1/-/-	-	0.4429	-	-	-
3-30/1-33	11	-	75	1/-/-	-	0.8233	-	-	-
3-30/3-11	10	-	80	1/-/-	-	0.4337	-	-	-

- Not determined due to insufficient material for assay

in a more complex disease relevant model of inflammation, Aldara-induced psoriasiform skin inflammation was utilized. In this model, the skin inflammation elicited by topical application of Aldara has been demonstrated to be mediated by IL25 [10, 11]. When mice were treated therapeutically with 22C7, after 3 days of Aldara treatment when mice had signs of skin inflammation, 22C7 significantly attenuated the development of inflammation. Animals treated with 22C7 had significantly reduced ear thickening and associated PASI score, with the decreased skin inflammation reflected in reduced epidermal thickness as well as immune cell infiltration after treatment with 22C7. These data taken in combination with the high affinity of 22C7 for IL25, demonstrates 22C7 efficacy in neutralization IL25-mediated Aldara-induced psoriasis skin inflammation when administered therapeutically to mice.

In the mouse air pouch model, the activity of 22C7 was shown to be dose dependent, whereas a single dose of mAb (20 mg/kg 22C7 injected IP every second day) was evaluated in the Aldara-induced psoriasis inflammation model. This dosing regime was selected to explore efficacy of 22C7, while minimizing the potential impact of target-mediated drug disposition. This treatment protocol demonstrated the efficacy of 22C7 in suppressing skin inflammation, with comparable activity as reported in another mouse study when we used a commercial mAb against mouse IL-25 (clone 35B; BioLegend, CA, USA) in the Aldara model [11]. Future work to determine the pharmacokinetic properties of 22C7 in mice is required to ensure optimal dosage regimes are used.

In this study, we have generated a potent anti-IL25 antibody, clone 22C7, with high affinity for mouse and human IL25. We have demonstrated the ability of 22C7 to neutralize the activity of IL25 *in vitro* and furthermore *in vivo* blocks IL25-mediated cellular responses in two distinct mouse models. As we had demonstrated using *in vivo* models of inflammation that 22C7 was functional in targeting IL25, we used a CDR-grafting approach to humanize 22C7. The humanization of the 22C7 clone has generated a graft, VH3-23/Vk1-39, which shows equivalent functional activity to the parental 22C7, and displaying the favorable developability characteristics required for therapeutic progression, including low predicted immunogenicity. The generation of this novel molecule that effectively blocks IL25-mediated inflammation has therapeutic potential for application in cancer, allergic, viral infections as well as inflammatory and auto-immune conditions.

## MATERIALS & METHODS

### Immunization and hybridoma generation of anti-IL25 antibodies

Mice were immunized with 20  $\mu$ g of recombinant human IL25 through IP injection with RIBI adjuvant on Days 1, 4, 8, 11, 24 and 31. To determine anti-IL25 titers, test bleeds were collected from the immunized animals and the anti-IL25 specific titers were determined by ELISA on human and mouse IL25 recombinant protein. The total B cell population from the immunized animals was isolated from splenocytes using the Milltenyi B cell isolation

kit. Isolated B cells were fused with P3X myeloma at 1:2 ratio using polyethylene glycol. Fused cells were plated at 2.5E10 cells per well in Excel-610 media supplemented with hypoxanthine-aminopterin-thymidine and 10% fetal bovine serum. Resulting hybridomas were screened for anti-human and mouse IL25 reactivity using hybridoma supernatant by ELISA.

### Humanization

22C7 murine CDR sequences were grafted onto human germline V-gene frameworks selected from the IMGT database based primarily on sequence identity (IGHV3-7, IGHV3-23, IGHV3-30, IGHV4-30-4, IGHV4-39, IGHV4-59, IGKV1-33, IGKV1-39, IGKV3-11). V-genes were synthesized at Blue Heron and sub-cloned into IgG expression vectors.

### IgG expression

HEK-293 Expi™ cells were transfected with IgG expression plasmids and ExpiFectamine transfection reagent (Gibco) as per manufacturer's instructions. Cell media was harvested 5 days post-transfection and purified using the Phynexus MEA robot using ProPlus ProA resin tips. Purified IgGs were buffer exchanged into phosphate-buffered saline (PBS) and quantified on a NanoDrop 2000 spectrophotometer.

### IgG binding ELISA

Nunc 96-well Maxisorp plates were coated overnight with 100  $\mu$ L of 1  $\mu$ g/ml human IL25 recombinant protein (R&D systems) diluted in PBS, pH 7.4 at 4°C. Coated plates were washed five times with 300  $\mu$ L of wash buffer (PBS, 0.02% Tween) and blocked in 200  $\mu$ L of 1% Casein block (Sigma) for 1 h. A 4-fold dilution series of a 400 nM stock IgG in was prepared using blocking solution as diluent, and 100  $\mu$ L of each dilution was added to the blocked plate for 1 h at room temperature. The washing step was repeated, followed by incubation with a secondary antibody for 1 h (horseradish peroxidase-conjugated anti-human IgG at 1/2 000 dilution in block (Jackson ImmunoResearch, cat# 109-035-008). Plates were washed and developed using 75  $\mu$ L Tetramethylbenzidine (TMB) and with subsequent addition of 75  $\mu$ L 0.18 M phosphoric acid to stop the reaction. Plates were read on the Envision plate reader (Perkin-Elmer) at absorbance 450 nm and data were plotted using GraphPad Prism, version 9.0.0 (121) (GraphPad Software Inc.).

### Analytical SEC

IgGs were diluted to 0.5 mg/ml in 200 mM sodium phosphate, 400 mM NaCl, pH 7.2 and analyzed on an Agilent 1200 HPLC with a YMC 200-Diol column to monitor for the presence of aggregates and determine the % POI content.

### Capillary differential scanning calorimetry (VP-DSC)

Antibody thermal stability was analyzed using Malvern's capillary VP-DSC equipped with an autosampler. The antibody sample prepared at 0.02 mM in PBS buffer

was placed in the sample cell with PBS buffer in the reference cell and heated from 10°C to 100°C at a scan rate of 100°C/h. The heat capacity difference between the sample cell and reference cell was recorded and analyzed using Origin 7.0 software from Malvern. A buffer-only baseline thermogram was generated and the data were used to subtract any system heat not associated with protein denaturation.

### Biophysical analysis

Purified IgGs were analyzed in ELISA format in a high-throughput automated workflow for binding to DNA and insulin against in-house controls, as previously described (Avery *et al.* 2018). A similarly high-throughput method was used for IgG assessment in the AC-SINS using purified IgGs at a concentration of 1 mg/mL as previously described (Avery *et al.* 2018).

### In silico assessment of immunogenicity

Antibody VH and VL region sequences were analyzed using EpiMatrix (Epivax) [16]. Each variable region was constructed into overlapping 9-mer peptides with each peptide overlapping the previous peptide by eight amino acids. Each 9-mer peptide was scored for predicted binding to each of eight HLA Class II alleles (DRB1\*0101, DRB1\*0301, DRB1\*0401, DRB1\*0701, DRB1\*0801, DRB1\*1101, DRB1\*1301, and DRB1\*1501). Peptides which score above 1.64 on the EpiMatrix "Z" scale are classed as a "hit" for binding to the predicted major histocompatibility complex molecule (~5% of a peptide set will score as a hit). Peptides scoring four or more "hits" from the eight alleles are classified as predicted T-cell epitopes and inform the Epivax score.

### BIAcore

SPR was used to determine binding kinetics of antibodies on a BIAcore T200 machine. A CM5 chip was prepared by immobilization of 9 000–13 000 RU of Fab capture reagent, as per manufacturer's protocol (Cytiva, Human Fab Capture Kit). IgGs were prepared in HBS-EP+ buffer (0.01 M HEPES, 0.15 M NaCl, 3 mM ethylenediaminetetraacetic acid (EDTA) and 0.05% (v/v) surfactant P20, pH 7.4) and injected for 60 s at a flow rate of 10  $\mu$ L/min aiming for a coating level of 100 RU of IgG. Human or mouse IL25 was prepared in HBS-EP+ buffer in a 2-fold dilution series from 25 nM to 0.78 nM and injected for 120 s at a flow rate of 100  $\mu$ L/min followed by a dissociation time of 180–600 s. The surface was regenerated with 10 mM glycine-HCl pH 2.1 injected at 10  $\mu$ L/min, for 25 s. All experiments were performed at 37°C. Sensorgrams were double referenced with buffer injections. Rate constants were determined by applying a 1:1 Langmuir binding model using the BIAevaluation software for determining the equilibrium dissociation constant with the equation  $KD = kd/ka$ .

### HT29 assay

Antibodies were evaluated for ability to inhibit IL17E signaling using the HT-29 cell line (ATCC). Cells (lot 60951991) were maintained in McCoy's 5A media (Gibco)

supplemented with 10% heat-inactivated FBS (Gibco), 100 U/ml penicillin and 100  $\mu$ g/ml streptomycin (Gibco) in 5% CO<sub>2</sub> at 37°C. Cells were passaged with 1:3–1:8 dilutions at 80–90% confluency two to three times/week. For the experiments, 30 000 cells were plated in 96-well, polystyrene, flat-bottomed tissue culture plates (Falcon) and left overnight in 5% CO<sub>2</sub> at 37°C. Titrations of experimental or control antibodies, rhIL17E pAb, rmIL17E mAb, rmIL17RB-Fc or rhIL-17RB-Fc (R&D Systems), were then added to the cells in fresh media and combined with spikes of either recombinant mouse or human IL25 (R&D Systems) to achieve 1.3 ng/ml IL25 in 150  $\mu$ L total volume. After ~19 h, cell supernatant was evaluated for GRO $\alpha$  content using ELISA (R&D Systems) according to the manufacturer's recommended protocol and reagents. IC<sub>50</sub>s were calculated using XLFit, version 5.4.0.8, 4 parameter equation #205 (IDBS) and graphical overlays were prepared using GraphPad Prism, version 9.0.0 (121) (GraphPad Software Inc.).

### Animals

C57BL/6 J strain mice (The Jackson Laboratory) were used at an age between 8 and 12 weeks. The animals were housed in a specific pathogen-free facility in individually ventilated and filtered cages under positive pressure. The animals had access to food and water *ad libitum*. All animal experiments were performed in compliance with the Irish Department of Health and Irish Health Products Regulatory Authority regulations (AE19136/P036 and AE19136/P077) and approved by Trinity College Dublin's BioResources ethical review board.

### Air pouch model

Air pouches were generated as previously described [19, 20]. Anaesthetized mice were injected with 5 mL sterile air subcutaneously into the back. The air pouch was reinflated with 3 mL sterile air after 3 days. At Day 5, mice were injected with 0.5 mL of PBS or 0.5 mL of rmIL25 (500 ng) in PBS. The PBS-only group was re-injected immediately with an additional 0.5 mL PBS into the air pouch. Groups of mice that received recombinant mIL25 were also injected with 0.5 mL PBS, isotype control antibody (1 000 ng of anti-*Eimeria tenella* IgG2a in PBS), 22C7 (250 ng in 0.5 mL PBS) and 22C7 (1 000 ng in 0.5 mL PBS). After 24 h, mice were culled, and lavage solution (PBS with 5.4 mM EDTA) was injected into the air pouch and recovered. The air pouch lavage fluid was centrifuged at 400 *g* for 10 min at 4°C, before the cells were counted and processed for flow cytometry, as below.

### Aldara model of psoriasis-like inflammation

The protocol for the Aldara-induced mouse model of psoriasis-like inflammation has been published previously [21, 22]. Mice received Aldara cream (5% w/w imiquimod, MEDA Pharmaceuticals) or Vaseline on right or left ear, respectively, daily for up to 12 consecutive days. Starting on Day 3 when mice had signs of erythema, and then every other day, mice received IP injection (20 mg/kg body weight) of 22C7 or anti-*E. tenella* isotype control antibody.

The diameter of ears of mice was measured daily with a thickness gauge micrometer (Mitutoyo No 7309). The ears of mice were scored daily for signs of psoriasis-like inflammation using a mouse PASI system. The ears were scored according to three parameters: erythema, thickening and scaling. For each parameter, the mice were scored on a scale from 0 to 4: Erythema was scored 0–4 on the degree of redness of the skin; thickening was extrapolated from increase in ear thickness < 10% 0, 10–25% 1, 25–50% 2, 50–75% 3 and > 75% 4; scaling scored 0, mild pathology scored 1, moderate pathology 2, marked pathology 3 and very severe pathology a score of 4. The total cumulative score of all three parameters was up to a maximum of 12.

### Histology

Mouse ear tissue was fixed in 10% formaldehyde saline. Paraffin-embedded sections were cut, and slides were stained with hematoxylin and eosin. Slides were scanned, at  $\times 20$  original magnification, using an Aperio ScanScope and ImageSoftware (Leica Biosystems Ltd). The epidermal thickening was measured in  $\mu$ m at 20 different locations along the length of each ear sample. The number of infiltrating cells found in a 2 500  $\mu$ m<sup>2</sup> field of the dermis was counted at 10 different locations along the section. The average number of infiltrating cells was calculated for each mouse.

### Flow cytometry

Cells recovered from air pouches were counted and resuspended in block containing anti-mouse CD16/CD32. Cells were stained anti-Siglec F-APC (Clone: 1RN44N, Invitrogen), anti-CD11b-APC-Cy7 (Clone: M1/70, Biolegend), anti-CD3/anti-CD19-BV421 (Clone CD3: 17A2, Biolegend; Clone CD19: eBio1D3 (1D3), Invitrogen), anti-Ly6G-BV650 (Clone 1A8, Biolegend), anti-CD45-BV711 (Clone: 30-F11, Biolegend) and anti-CD11c-PE (Clone: HL3, BD Pharmingen). A live/dead marker (Live/Dead Aqua; Thermo Scientific) was included to ensure analysis of viable cells only. Cells were acquired using a BD LSR Fortessa flow cytometer (BD Biosciences) followed by analysis with FlowJo software.

### Statistics

Statistical analysis was performed using Graph Pad Prism software (version 9.0.1). Results are presented as dots for individual animals together with the mean  $\pm$  standard error of the mean (SEM), as mean  $\pm$  SEM for time course graphs or as bar charts for calculations of the area under the curve (AUC). Statistical significances calculated using the Student's *t* test were depicted as follows:

\* equals  $p \leq 0.05$ , \*\*equals  $p < 0.01$  and \*\*\*equals  $p < 0.001$ .

### ABBREVIATIONS

AC-SINS	affinity-capture self-interaction nanoparticle spectroscopy
CDRs	complementarity determining regions
DNA	deoxyribonucleic acid

EC50	half maximal effective concentration
EDTA	ethylenediaminetetraacetic acid
ELISA	enzyme-linked immunosorbent assay
Gro $\alpha$	growth-regulated oncogene alpha
HEK-293	human embryonic kidney –293
HRP	horseradish peroxidase
IC <sub>50</sub>	half maximal inhibitory concentration
IgE	immunoglobulin class E
IgG	immunoglobulin class G
mAbs	monoclonal antibodies
nM	nanomolar
pAB	polyclonal antibody
PBS	phosphate-buffered saline
POI	peak of interest
pM	picomolar
SDS-PAGE	sodium dodecyl sulphate–polyacrylamide gel electrophoresis
SEC	size exclusion chromatography
VH	variable heavy
VL	variable light

## SUPPLEMENTARY DATA

Supplementary Data are available at ABT Online.

## ACKNOWLEDGEMENTS

We thank May Tam, Chris Corcoran, Liz DiBlasio-Smith, Karl Malakin and Ed LaVaille for the preparation of IL25 reagents. We thank Sybille Moesta for carrying out the DSC experiments. The authors thank Edwina Stack, Virginia McManus, Khetemnee Lam, Sarah Parotta and Lily Zhu for the generation of IL17RB-Fc and Darren Ferguson for the preparation of anti-*E. tenella* IgG2a.

## FUNDING DETAILS

This study was funded by Science Foundation Ireland (14/BIAP/B2959).

## DISCLOSURE OF POTENTIAL CONFLICTS OF INTEREST

Ruth Bone, Brian Fennell, Amy Tam, Richard Sheldon, Karl Nocka, Chew Shun Chang, Sreeja Varghese and Orla Cunningham are all past or present employees of Pfizer Inc.

## DATA AVAILABILITY STATEMENT

The data underlying this article will be shared on reasonable request to the corresponding author.

## ETHICS AND CONSENT STATEMENT

Consent was not required.

## ANIMAL RESEARCH STATEMENT

All animal experiments were conducted in compliance with EU legislation on the protection of animals used for scientific purpose (Directive 2010/63/EU).

## REFERENCES

- McGeachy, MJ, Cua, DJ, Gaffen, SL. The IL-17 family of cytokines in health and disease. *Immunity* 2019; **50**: 892–906.
- Prinz, I, Sandroch, I, Mrowietz, U. Interleukin-17 cytokines: effectors and targets in psoriasis—a breakthrough in understanding and treatment. *J Exp Med* 2020; **217**: e20191397.
- Lee, J, Ho, WH, Maruoka, M *et al.* IL-17E, a novel proinflammatory ligand for the IL-17 receptor homolog IL-17Rh1. *J Biol Chem* 2001; **276**: 1660–4.
- Fort, MM, Cheung, J, Yen, D *et al.* IL-25 induces IL-4, IL-5, and IL-13 and Th2-associated pathologies in vivo. *Immunity* 2001; **15**: 985–95.
- Borowczyk, J, Shutova, M, Brembilla, NC *et al.* IL-25 (IL-17E) in epithelial immunology and pathophysiology. *J Allergy Clin Immunol* 2021; **148**: 40–52.
- Fallon, PG, Ballantyne, SJ, Mangan, NE *et al.* Identification of an interleukin (IL)-25-dependent cell population that provides IL-4, IL-5, and IL-13 at the onset of helminth expulsion. *J Exp Med* 2006; **203**: 1105–16.
- Mullard, A. FDA approves first-in-class TSLP-targeted antibody for severe asthma. *Nat Rev Drug Discov* 2022; **21**: 89.
- Gauvreau, GM, White, L, Davis, BE. Anti-alarmin approaches entering clinical trials. *Curr Opin Pulm Med* 2020; **26**: 69–76.
- Ballantyne, SJ, Barlow, JL, Jolin, HE *et al.* Blocking IL-25 prevents airway hyperresponsiveness in allergic asthma. *J Allergy Clin Immunol* 2007; **120**: 1324–31.
- Xu, M, Lu, H, Lee, YH *et al.* An Interleukin-25-mediated autoregulatory circuit in keratinocytes plays a pivotal role in psoriatic skin inflammation. *Immunity* 2018; **48**: 787–798.e4.
- Senra, L, Mylonas, A, Kavanagh, RD *et al.* IL-17E (IL-25) enhances innate immune responses during skin inflammation. *J Invest Dermatol* 2019; **139**: 1732–1742.e17.
- Camelo, A, Barlow, JL, Drynan, LF *et al.* Blocking IL-25 signalling protects against gut inflammation in a type-2 model of colitis by suppressing nuocyte and NKT derived IL-13. *J Gastroenterol* 2012; **47**: 1198–211.
- Williams, TC, Loo, S-L, Nichol, KS *et al.* IL-25 blockade augments antiviral immunity during respiratory virus infection. *Commun Biol* 2022; **5**: 415.
- Jain, T, Sun, T, Durand, S *et al.* Biophysical properties of the clinical-stage antibody landscape. *Proc Natl Acad Sci U S A* 2017; **114**: 944–9.
- Avery, LB, Wade, J, Wang, M *et al.* Establishing in vitro in vivo correlations to screen monoclonal antibodies for physicochemical properties related to favorable human pharmacokinetics. *MAbs* 2018; **10**: 244–55.
- Schafer, JR, Jesdale, BM, George, JA *et al.* Prediction of well-conserved HIV-1 ligands using a matrix-based algorithm, EpiMatrix. *Vaccine* 1998; **16**: 1880–4.
- Smith, AD, Fan, A, Qin, B *et al.* IL-25 treatment improves metabolic syndrome in high-fat diet and genetic models of obesity. *Diabetes Metab Syndr Obes* 2021; **14**: 4875–87.
- Deng, C, Peng, N, Tang, Y *et al.* Roles of IL-25 in type 2 inflammation and autoimmune pathogenesis. *Front Immunol* 2021; **12**: 691559.
- Smith, P, Mangan, NE, Walsh, CM *et al.* Infection with a helminth parasite prevents experimental colitis via a macrophage-mediated mechanism. *J Immunol* 2007; **178**: 4557–66.
- Ludwig, A, Otto, GP, Riento, K *et al.* Flotillin microdomains interact with the cortical cytoskeleton to control uropod formation and neutrophil recruitment. *J Cell Biol* 2010; **191**: 771–81.
- Russell, SE, Stefanska, AM, Kubica, M *et al.* Toll IL-1R8/single Ig IL-1-related receptor regulates psoriasisform inflammation through direct inhibition of innate IL-17A expression by gammadelta T cells. *J Immunol* 2013; **191**: 3337–46.
- Hernandez-Santana, YE, Leon, G, St Leger, D *et al.* Keratinocyte interleukin-36 receptor expression orchestrates psoriasisform inflammation in mice. *Life Sci Alliance* 2020; **3**: e201900586.